TRANSPORT PROBLEMS 2026 Volume 21 Issue 1
PROBLEMY TRANSPORTU DOI: 10.20858/tp.2026.21.1.03

Keywords: hot-air balloon; CFD; airflow; drag coefficient

Vitaly DUDNIK[1]*, Wawrzyniec PANFIL[2], Wojciech MOCZULSKI[3], Robert ŻBIKOWSKI[4], Yevhenii SHKVAR[5]

AN INVESTIGATION OF A HOT-AIR BALLOON HORIZONTAL MOTION IN CONDITIONS OF A HORIZONTAL THRUST FORCE APPLICATION

Summary. Balloons perform flights during which they can transport passengers and equipment over considerable distances. However, one problem associated with these aircraft is landing in confined areas, particularly in densely populated regions of Europe or mountainous terrain, where the number of suitable landing sites is limited. Installing a propulsion system equipped with a propeller generating thrust in the horizontal plane is a feasible way to solve this problem. General data which need for propulsion system investigated in this work. A computational fluid simulation of balloon aerodynamics and an experiment with a full-scale balloon were conducted to determine the required propulsion system parameters for installation on the balloon basket. During the research, the balloon's aerodynamic drag was determined, the influence of balloon deformation on flight dynamics was assessed, and the maximum wind speed that the balloon could withstand when equipped with the propulsion system was identified. Modeling the dynamics of the balloon's motion based on experimental results made it possible to determine the aircraft's response time to propulsion system activation. In particular, the influence of different values of propulsive thrust on the behavior of the balloon was investigated.

1. INTRODUCTION

Balloons possess several specialized and unique properties that define their application areas. These aircraft are commonly used for atmospheric sounding, meteorological and astronomical research, as well as for carrying airborne radar systems, telecommunication equipment, and other specialized devices.

Balloons and airships may play a significant role in the exploration of other planets. Numerous proposals have been made regarding the application of robotic balloons for extraterrestrial atmospheric flights associated with planetary exploration [3]. For instance, several studies have suggested utilizing robotic balloons to explore Titan, Saturn's largest moon [10, 11]. Additionally, various organizations routinely use radiosondes carrying sensors to stratospheric altitudes; these balloons burst at predetermined altitudes when the film stretches beyond their elastic limits and subsequently return to Earth by means of deployable parachutes [1].

[1] Silesian University of Technology, Faculty of Mechanical Engineering; Konarskiego 18A, 40-100 Gliwice, Poland; e-mail: vitaly.dudnik@polsl.pl; orcid.org/0000-0002-5798-8019
[2] Silesian University of Technology, Faculty of Mechanical Engineering; Konarskiego 18A, 40-100 Gliwice, Poland; e-mail: wawrzyniec.panfil@polsl.pl; orcid.org/0000-0001-7304-554X
[3] Silesian University of Technology, Faculty of Mechanical Engineering; Konarskiego 18A, 40-100 Gliwice, Poland; e-mail: wojciech.moczulski@polsl.pl; orcid.org/0000-0002-4697-1561
[4] Private company; Wybickiego 21, 57-340 Duszniki-Zdrój, Poland; e-mail: zbiki@wp.pl; orcid.org/0009-0006-6460-4737
[5] Zhejiang Normal University, College of Engineering of the Zhejiang Normal University; 688, Yingbin Road, Jinghua, 321004 Zhejiang, China; e-mail: shkvar.eugene@qq.com; orcid.org/0000-0001-9589-5860
* Corresponding author. E-mail: vitaly.dudnik@polsl.pl

Stratospheric balloons can also be designed for the long-range and long-duration transportation of payloads. The work [12] analyzed heat and mass parameters required for sustained, controlled-velocity flights. Surprisingly, it may be feasible to use balloons to transport large payloads at nearly constant altitudes for extended periods (e.g., several weeks) during the Antarctic summer. Another notable application involves transporting people for recreational or sporting events, as balloons can carry passengers over considerable distances. However, one significant issue with these aircraft is that they are difficult to land in confined areas, particularly in densely populated regions of Europe or in mountainous areas, where suitable landing sites are limited. One way to solve this problem could be to use propulsion drives including an electric motor and a propeller. Research in this direction was conducted more than 50 years ago [13] but was not implemented in practice. Currently, propeller propulsion drives have been developed by FlyDOO [21]. Interesting research on the lateral motion of a balloon was presented by Daidzic [8]. However, he did not investigate the dimensionless drag coefficient of a balloon during sliding. As a result, practically speaking, there are no reliable data on the aerodynamic drag and behavior of a hot-air balloon in horizontal movement, which would enable the design and optimization of propulsion drives for balloons.

With this problem in mind, the objective of this research is to study the possibility of using a propulsion power plant on a balloon and examine the factors influencing horizontal forced movement. The following tasks were completed to achieve this objective:

- assessing aerodynamic drag of the balloon,
- evaluating the influence of balloon deformation on flight dynamics,
- identifying the maximum wind speed that the balloon can withstand while equipped with the propulsion system.

The modeling of the balloon's aerodynamics and an experiment with a real balloon were performed to accomplish these tasks.

An electric power plant with a propeller creating thrust in the horizontal plane can be used as a propulsion system in the future. Such a propulsion system could halt the balloon's motion in windy conditions or move it toward a suitable landing site if the balloon initially misses the landing zone. This does not mean that the drive is designed for a full-fledged fight against the wind. The main idea is to correct the position of the balloon in cases when the landing calculation has already been made by the pilot and a sharp correction is required. Such a mode may require the application of maximum propulsive thrust and the flight of the balloon at maximum speed for a limited time of less than one minute. It should be taken into account that the maximum airspeed of the balloon cannot be very high (it is usually about 3 m/s). If the wind has a higher speed than this, the balloon will move with it. Additionally, the presence of this propulsion system allows horizontal maneuvering to avoid collisions with other balloons and facilitates entry into localized upward air currents.

Traditionally, lighter-than-air vehicles equipped with propulsion systems are classified as airships. However, in this scenario, the balloon cannot be considered a full-fledged airship, as the propulsion system is designed only for short-term, limited activation. In some cases, the propulsion system can be used for a prolonged horizontal flight of up to 30 minutes with a lower speed of 1–2 m/s and lower energy consumption. It makes no sense to design the power plant for a longer flight, as this would increase the balloon's weight and decrease its carrying capacity. Thus, the main planned altitude for using the power plant is the ground layer (less than 1 km).

2. EXPERIMENTAL BALLOON

A hot-air balloon with a maximum horizontal diameter of 14 m and a volume of 1840 m³ was used for the experimental tests. During experiments, wind speeds ranged from 0.6–1.2 m/s, according to measured data. Zero-velocity flight measurements were carried out during neutral buoyancy low-altitude balloon flights. A basket containing liquefied gas tanks, a pilot, and passengers was attached beneath the balloon. A burner was installed on top of the basket. The pilot regulated the vertical motion by adjusting the air temperature in the balloon by activating the gas burner. Thus, vertical climb and

descent were controlled by the pilot without introducing additional lateral forces, with horizontal motion determined primarily by wind direction.

The balloon's system masses utilized during the experiment are summarized in Table 1. The payload during the experiment consists of a pilot and one passenger. Fig. 1a is a photo of the balloon during testing. Data analysis was facilitated by side-projection video footage of the balloon's movements. An autopilot equipped with an inertial measuring unit and a satellite navigation system receiver running on ArduPilot firmware was used to measure linear accelerations, rotary accelerations, position and velocity. The airfield anemometer data were combined with the ground speed data to determine the basket airspeed. The onboard anemometer data were used by the pilot primarily to control the balloon in level flight. An ArduPilot and an anemometer Habotest HT625A were installed in the balloon basket. Another anemometer was located on the airfield to monitor the wind conditions at the height of the basket. Several people applied muscle power by pulling a rope connected to the basket through a load cell to induce balloon motion. This allowed us to simulate the horizontal flight of the balloon near the ground. The following parameters were recorded during the experiment:

- force on the rope,
- airspeed,
- tilt angles of the basket,
- GPS coordinates,
- linear accelerations.

The locations of the measuring devices are indicated in Fig. 1b. The propulsion force was applied to the basket through the load cell (3); the instrumentation system and data recorder (2), based on ArduPilot, were also mounted on the basket. The anemometer (1) was continuously monitored by the crew.

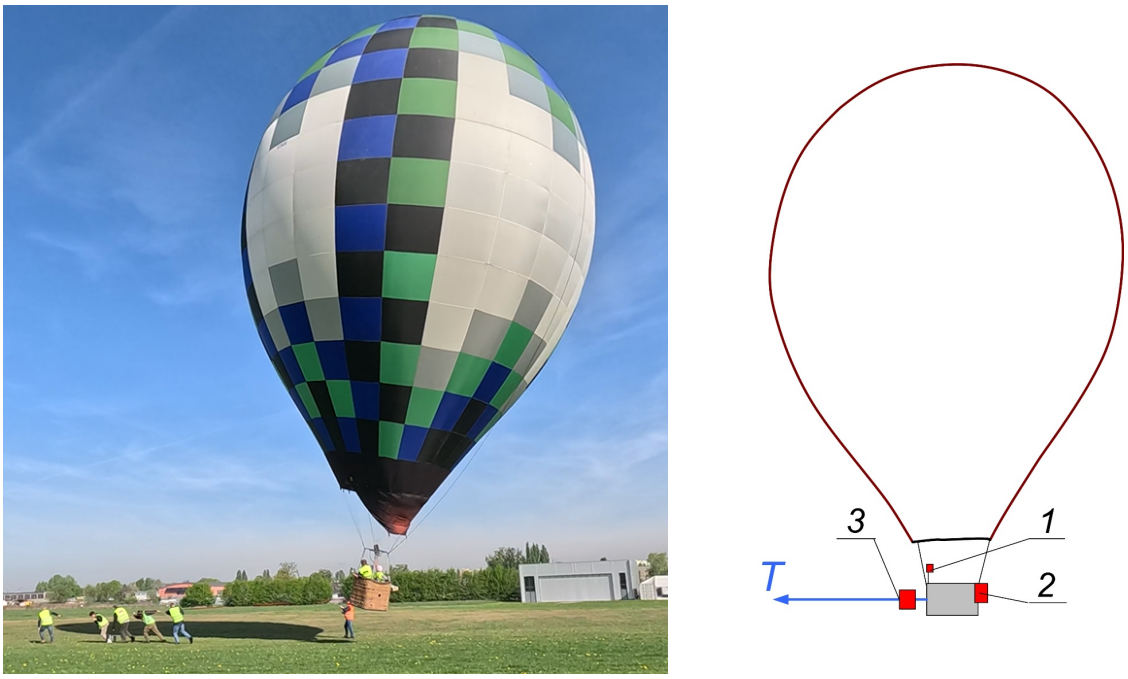

(a) (b)

Fig. 1. Performing the experiment (a) and the locations of measuring devices on the balloon (b): 1 – anemometer, 2 – instrumentation system and data recorder, 3 – load cell

The load applied to the balloon by the rope was measured using an AXIS H3 C3 loadcell connected directly to the rope. This load cell was capable of measuring up to 2000 N at a sampling rate of 2 Hz, with an accuracy of 0.1% of full scale (±2 N). The data were recorded on the SD card in the measuring device.

Table 1

Balloon System Masses

No.	Element	Mass (kg)
1	Balloon Envelope	96
2	Crew	155
3	Basket	74
4	Measuring System	2
5	Burner	24
6	Fuel System	78
	Total	429

3. SIMULATION-BASED DETERMINATION OF BALLOON DRAG COEFFICIENT

The drag of the balloon in cross flow is a key parameter for determining the horizontal thrust required from the actuator. Since the problem associated with the airflow around a balloon filled with internally heated air and accounting for the deformed shape has not been previously addressed, analytical drag estimation must rely on comparison with similarly shaped objects. In particular, studies involving high-pressure balloons [17, 19, 20] and spherically shaped objects were considered.

Existing methods for determining drag evaluate the drag coefficient of a spherically shaped object as a function of the Reynolds number. When the Reynolds number is sufficiently high, variations in the drag coefficient become minimal. For example, the formula approximating the empirical relationship of the ball drag coefficient (1) [2, 14] shows that the drag stabilizes at around 0.14 for high Reynolds numbers. A nearly identical value has also been reported in theoretical studies involving large-diameter spherical balloons [9].

$$C_d = \frac{24}{Re} + \frac{2.6\left(\frac{Re}{5.0}\right)}{1+\left(\frac{Re}{5.0}\right)^{1.52}} + \frac{0{,}411\left(\frac{Re}{2.63\times10^5}\right)^{-7.94}}{1+\left(\frac{Re}{2.63\times10^5}\right)^{-8.0}} + \frac{0.25\left(\frac{Re}{10^6}\right)}{1+\left(\frac{Re}{10^6}\right)} \quad , \tag{1}$$

where:

C_d – drag coefficient,

Re – Reynolds number.

However, the nature of the pear-shaped balloon examined in this study differs from that of classical spherical ones, and this difference can significantly affect the aerodynamic drag. Nevertheless, once the Reynolds number reaches $Re = 1 \times 10^6$, the drag coefficient should stabilize to some constant that can be determined theoretically and validated through experimental data.

The air surrounding the flying balloon can be treated as an incompressible viscous flow. The continuity and momentum equations in Cartesian coordinates are given by Equations (2) and (3) [20].

$$\frac{\partial u_j}{\partial x_j} = 0, \tag{2}$$

$$\frac{\partial u_i}{\partial t} + u_j \frac{\partial u_i}{\partial x_j} = -\frac{1}{\rho}\frac{\partial P}{\partial x_i} + \nu\nabla^2 u_i + \frac{\partial \sigma_{ij}}{\partial x_j} \quad , \tag{3}$$

where:

v – averaged local flow speed (m/s),

$i, j = \{1,2,3\}$ – indices, associated with the Cartesian coordinates $\{x_1, x_2, x_3\}$,

P – pressure (Pa),

ν – kinematic air viscosity (m^2/s),

ρ – air density (kg/m^3),

t – time (s),

σ_{ij} – additional Reynolds stresses, traditionally defined in accordance with the Reynolds approach through correlation of the product of pulsating components of velocity u'_m, m=i,j, so $\sigma_{ij} = -\overline{u'_i u'_j}$,

$\nabla^2() = \frac{\partial^2()}{\partial x_j \partial x_j}$ – the Laplacian.

Typically, unsteady Reynolds averaged Navier–Stokes equations are used to solve this type of problem. Solving the equations for each cell enables the determination of flow parameters in the vicinity of the balloon. However, in the present case, the problem is more complex, as the balloon does not have a rigid external shape—its geometry can deform under the influence of dynamic pressure. To accurately capture this effect, we must solve the governing equations in conjunction with the heat balance equations and the internal flow field of the heated air motion within the balloon. However, this approach can introduce errors, especially under complex, multidirectional flow conditions. Moreover, its implementation demands substantial computational resources [7]. Therefore, we decided to conduct the experiments using a full-scale balloon. Complementary flow simulations were also performed using ANSYS software to better interpret the experimental data and anticipate potential flow phenomena affecting the balloon. A computational unstructured mesh composed of tetrahedral elements was developed through the second-order finite element method, covering a rectangular parallelepiped domain. The final mesh comprised 3,076,510 elements, with a strong refinement in the vicinity of the balloon surface. This ensured numerical solution independence from mesh geometry and parameters.

The boundary conditions were set as follows: the velocity at all the outer surface faces of the computational domain, excluding the back face, was defined as for an inlet by the constant streamwise $\bar{v}_1$ component, equal to the undisturbed flow speed $\bar{v}_1 = U_\infty$, together with zero normal and transversal components $\bar{v}_2$=$\bar{v}_3$=0; the turbulence intensity was 0.05% of U_∞; the gauge pressure at the back face (outlet) was equal to zero; together with the absence of velocity gradients in the normal to this face direction, the streamlined surface of the balloon was simulated as an impermeable wall with the use of the no-slip condition $\bar{v}_1$=$\bar{v}_2$=$\bar{v}_3$=0.

The 2-equation shear stress transport (SST) version of the k-omega turbulence model was applied to calculate σ_{ij}, as it is the best-adapted model for the flow region near a streamlined surface.

The streamline behavior at high horizontal flight speeds was of particular interest. The horizontal airflow was analyzed across several cross-sections (Fig. 2). The simulation employed a simplified model that did not account for the vertical movement of hot air in the lower part of the balloon. Instead, only the horizontal surface in the lower region was considered. The sharp edge of the bottom tip in the balloon model induced localized turbulence and flow separation that is likely more pronounced in simulation than in a real balloon.

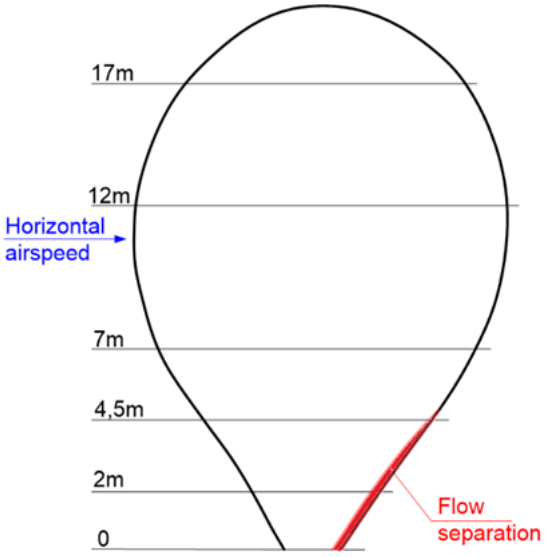

Fig. 2. Balloon sections presented in the simulation results

In the upper part of the balloon, significant airflow is observed not only laterally but also from above (Fig. 3a). The middle zone of the balloon exhibits stable flow without any signs of separation (Figs. 3b and 3c). In contrast, the lower zone—approximately from a height of 5 m downward—shows consistent flow separation (Figs. 3d and 3e). However, this flow separation observed in the simulation is not expected to induce local deformation of the balloon. This is because the shape in this lower region is supported by load-bearing ribbons, which are under significant tension due to the weight of the basket, crew, burner, and fuel. Finally, as follows from the visualization results presented for the flow around the shape of the balloon in various cross-sections (Figs. 2 and 3), at the maximum horizontal velocity, the flow is significantly spatial, and its 3D separation zone is significantly smaller than was observed in similar two-dimensional bodies.

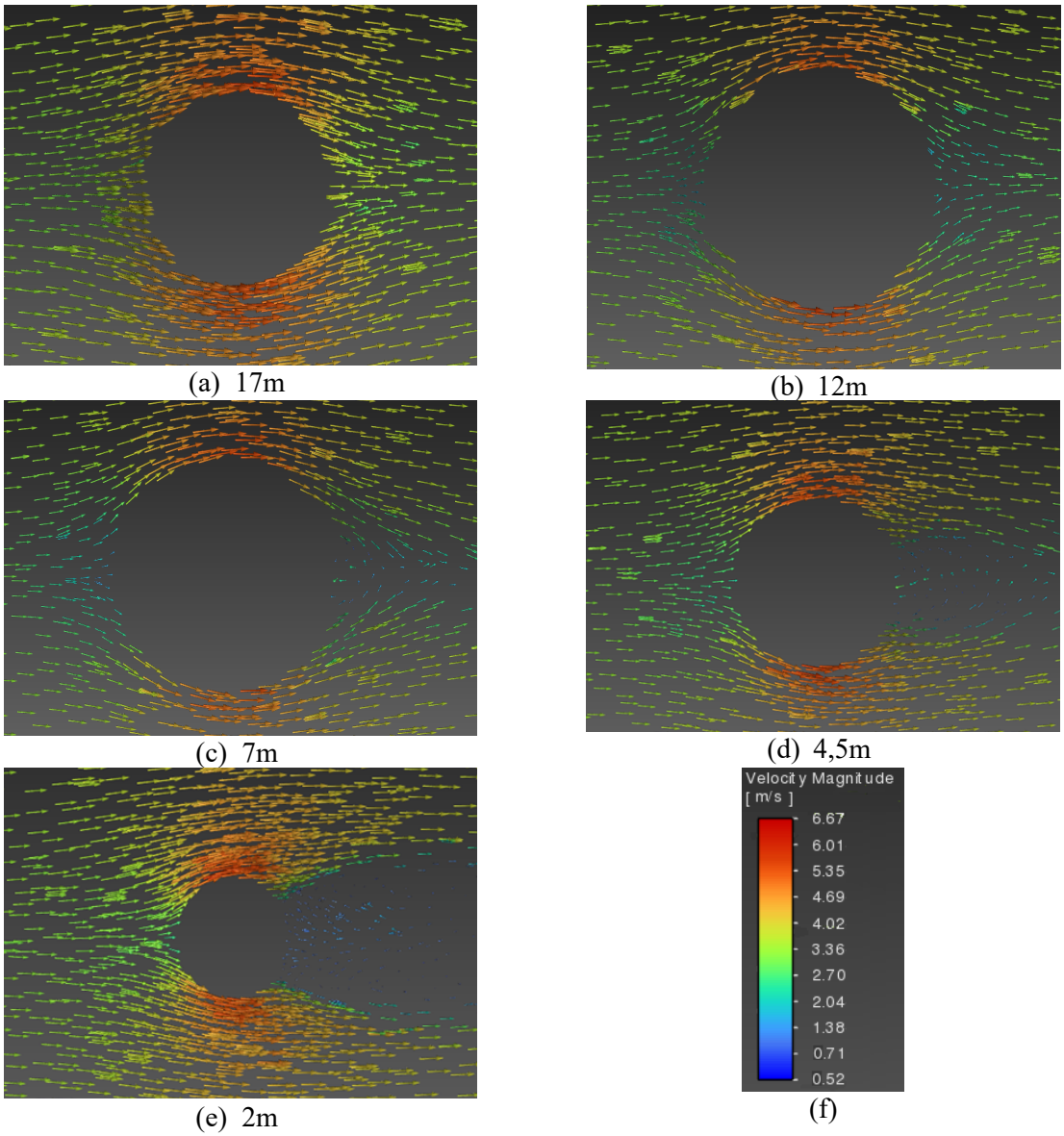

Fig. 3. The local airspeed distribution in the balloon sections according to height (a-e), with a legend (f)

Within the horizontal high-speed range of 3.0–3.5 m/s, the drag coefficient of the balloon was numerically estimated to be about 0.36 (Fig. 4). In reality, the balloon exhibits intensive internal airflow between the burner and the balloon envelope. As a result, the lower edge of the real balloon is less sharply defined, leading to more stable aerodynamic behavior and, consequently, a more consistent drag coefficient.

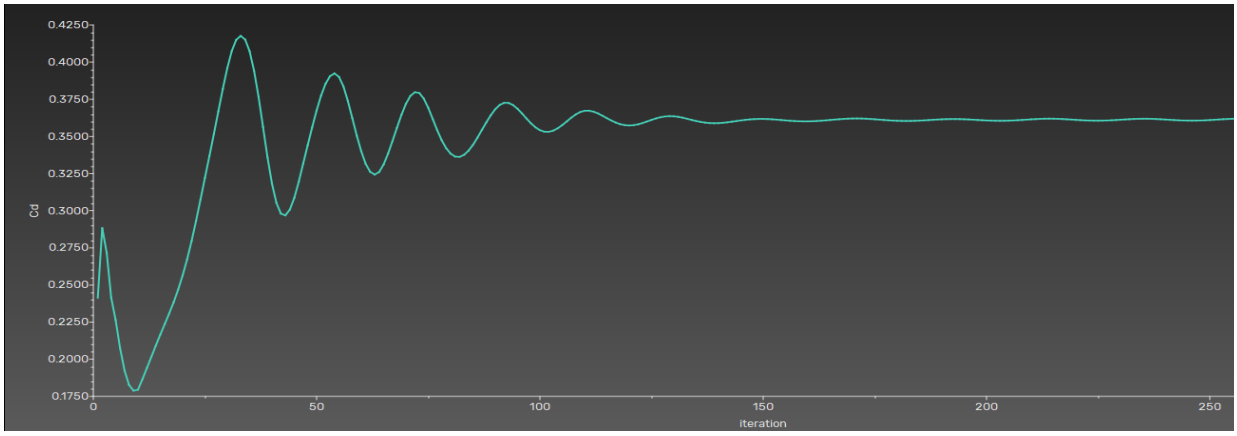

Fig. 4. Drag force coefficient according to the simulation results

4. EXPERIMENTAL RESULTS

During the experiment, the balloon and basket—two interconnected but freely suspended components in space—formed an oscillating system. When external forces are applied, the system needs time to stabilize its motion. Throughout the tests, the balloon was accelerated multiple times to its maximum airspeed. An example of the recorded force data is presented in Fig. 5. It can be seen that, despite the partial stabilization of the propulsive force after its application, the balloon continued to exhibit oscillatory motion before gradually reaching equilibrium.

The inclination of the balloon during motion caused the burner to direct its flame jet toward the balloon's inner wall. The maximum flight speed of the balloon was limited by the proximity of the flame to the envelope surface. Experimental observations indicate that the maximum safe airspeed at the basket altitude ranged from 2.9–3.0 m/s. Any further increase in horizontal velocity would have risked damaging the balloon's fabric due to heat exposure.

According to the recorded parameters, the average value of the maximum horizontal airspeed at the measuring point on the basket was $v_{bm\ max}$=2.92 m/s, and the average horizontal force was T=486N. In the steady-state mode of horizontal flight, the horizontal thrust produced by the propulsion system is equal to the drag force acting on the balloon, as expressed in Equation (4).

$$T = D_b + D_k = c_{db}\frac{\rho v_b^2}{2}A_{bv} + c_{dk}\frac{\rho v_b^2}{2}A_{kv}\ , \tag{4}$$

where:
T – horizontal propulsion thrust (N),
D_b – drag force of the balloon (N),
D_k – drag force of the basket (N),
c_{db} – drag force coefficient of the balloon,
c_{dk} – drag force coefficient of the basket,
v_b – horizontal airspeed of the balloon (m/s),
A_{bv} – area of vertical projection of the balloon (m^2),
A_{kv} – area of vertical projection of the basket (m^2).

The shape of the basket can be considered as a cubic body that moves in a position of 45 degrees between the lateral surfaces and the stream direction. According to [4], its drag force coefficient is 0.8, but since the basket has rounded corners, this value can be decreased to $c_{dk} = 0.6$. Thus, the basket's contribution to the drag of the whole system was determined to be $D_k = 7$ N.

The vertical cross-sectional area of the basket is significantly smaller than that of the balloon. Therefore, its aerodynamic drag is minimal.

One of the key challenges in analyzing the results of balloon experiments under wind conditions is the non-uniformity of airflow near the ground surface. During the tests, the height of the balloon's uppermost point ranged between 25 and 26 m, while wind speed measurements were taken at a height

of 2.5–3.5 m. The experiments were carried out in an open field, free of windward obstacles within at least 800 m of the wind side. Although the wind speed gradient was relatively small under these conditions, it was still present and had a measurable effect on the measured wind speed. According to [16], the wind speed in the surface layer can be expressed by the following relation:

$$w_h = w_m \frac{ln\, h - ln\, z_0}{ln\, h_m - ln\, z_0} \quad , \tag{5}$$

where:
w_h – horizontal speed of wind in the considered altitude (m/s),
w_m – horizontal speed of wind in the measurement point (m/s),
h – considered altitude (m),
h_m – altitude of measurements (m),
z_0 – surface roughness parameter.
Surface roughness can be defined through the dimensionless parameter *m*:

$$z_0 = 29.1m^2 - 6.8m + 0.4 \ . \tag{6}$$

In the standards of most European countries, the m parameter is considered [16] as:

$$m = \frac{1}{7} \ . \tag{7}$$

The results of these calculations demonstrate the significant influence of wind parameters on measurement outcomes, even under low wind speed conditions. For example, when the wind speed was w_m=1.20 m/s near the basket at a height of 2.5 m, the speed increased by 0.47 m/s at a height of 16 m, corresponding to the balloon's maximum diameter. This means the average airspeed of the balloon was v_b=3.39 m/s. Recalculating the data for this height showed a drag coefficient of c_{db}=0.35. This value enabled the estimation of the propulsion force required for other velocities.

Due to the balloon's large dimensions, the Reynolds number (Re) was high. For example, at a velocity of v_b=1.1 m/s, the Reynolds number already reached Re=1×10^6. At the maximum horizontal flight speed, the Reynolds number was Re=3.1×10^6. An analysis of published data from balloon-like objects indicates that the drag coefficient is relatively high at low Reynolds numbers [5, 6, 19]. However, once the Reynolds number exceeds approximately 1×10^5, the drag coefficient drops to a minimum value and remains nearly constant [19]. This means the received data will be applicable for all modes of the balloon's "high-speed" flights.

An important aspect of studying balloon behavior under horizontal force is to analyze changes in the balloon's shape. Most modern balloon envelopes are designed in so-called "natural shapes," which are characterized by virtually zero hoop stress. The vertical load bands, attached to the crown ring, support the weight of the entire system. The envelope fabric remains nearly fully tensioned, while a slight internal overpressure, generated by the heated lifting air relative to the cooler ambient atmosphere, maintains the envelope's form [18].

However, under horizontal airflow, the balloon does not behave like a rigid body and may undergo deformation due to dynamic pressure. Such deformation can reduce the internal volume, potentially causing air to escape through the lower orifice. This escaping air may generate a transient jet stream, producing a brief upward vertical thrust.

The principal concern, however, is related to the reduction of the balloon's internal volume, which directly decreases lift. To analyze potential changes in the balloon's shape and volume, side-by-side images were captured of the balloon, both at rest and during horizontal motion. The comparison results are presented in Fig. 6a. The blue contour corresponds to the balloon's shape under still-air conditions; the red contour illustrates its shape at maximum horizontal velocity.

The maximum reduction in the balloon's depth along the longitudinal axis was measured at 4.5%. Although the balloon's length decreased, the perimeter of the horizontal cross-section remained unchanged due to the continuity of the envelope fabric. In subsequent analyses, the horizontal cross-section at maximum airspeed was approximated by an elliptical shape. Under the condition of perimeter conservation, the minor and major axes of the equivalent ellipse were determined according to the following relation:

$$2\frac{\pi ab+a-b}{a+b} = \pi R\,, \tag{8}$$

where:
a – long semi-major axis of the horizontal cross-section of the balloon in the maximum horizontal airspeed flight mode (m),
b – short semi-major axis of the horizontal cross-section of the balloon in the maximum horizontal airspeed flight mode (m),
R – radius of the horizontal cross-section of the balloon without horizontal airspeed.

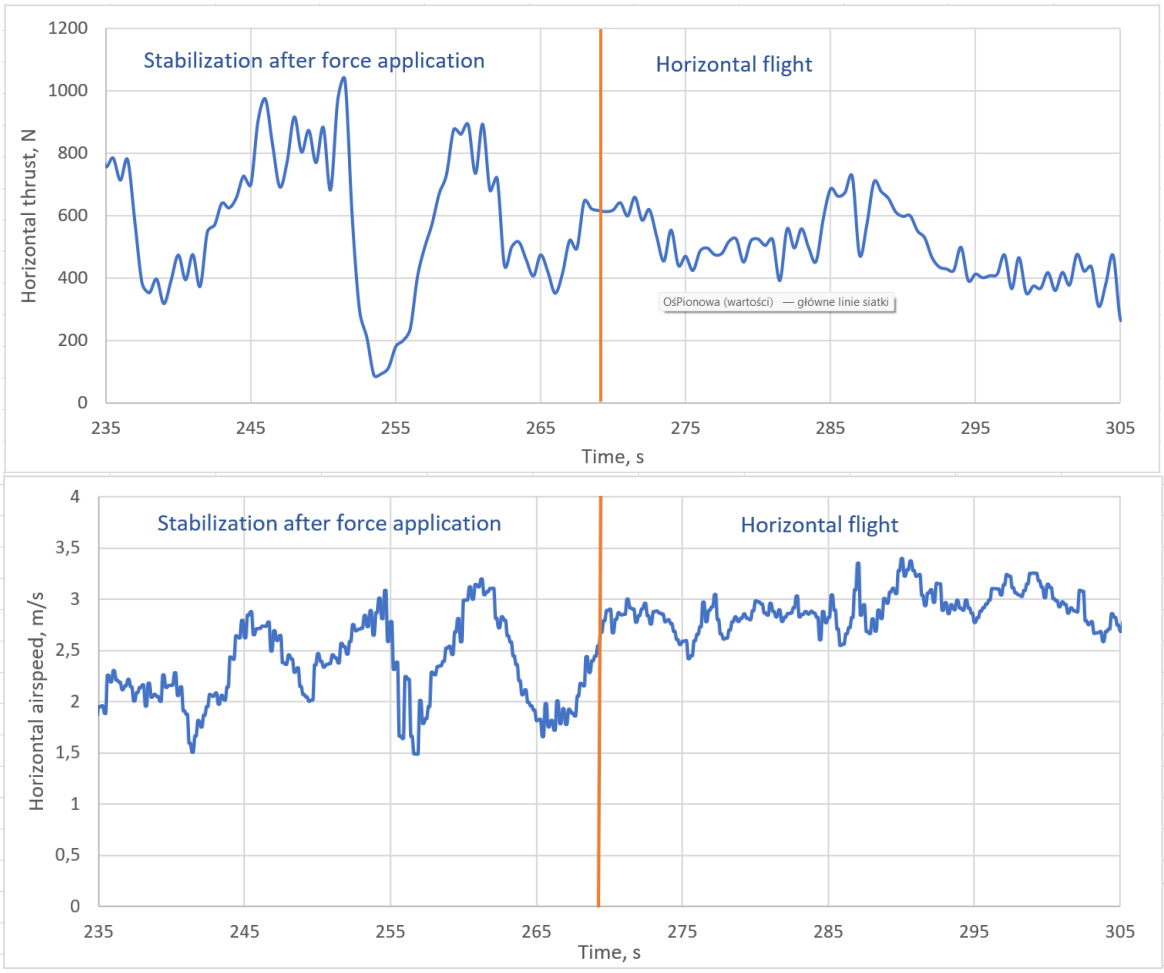

Fig. 5. Force and flight velocity parameters during the experiment

Accordingly, the cross-sectional area of the balloon at maximum flight speed was calculated based on the parameters of an elliptical shape, while under zero horizontal velocity, it was determined assuming a circular cross-section. For a constant perimeter, the area of an ellipse is smaller than that of a circle, which reduces the balloon's internal volume. The longitudinal deformation of the envelope, together with the variation in cross-sectional area as a function of height, is illustrated in Fig. 6b. The distribution of these parameters was used to compute the integrated volume of the balloon under dynamic flow conditions (9).

$$V_b = \int_0^H A_{bhi}\, dH \tag{9}$$

where:
V_b – volume of balloon (m^3),
H – height of balloon (m),
A_{bhi} – current horizontal section of balloon (m^2).

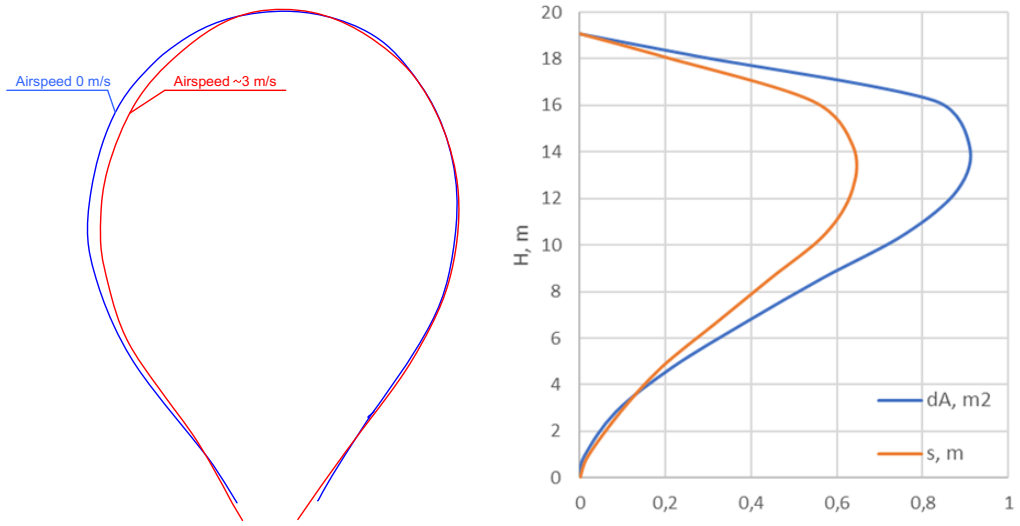

(a) (b)

Fig. 6. (a) Change of the balloon shape and distribution of the balloon deformation and (b) horizontal cross-sectional area by height during the flight with maximum horizontal velocity compared to the stopped balloon. The tilt of the balloon was not considered

The calculations indicate that the balloon's internal air volume decreased by 26.0 m³. This reduction corresponds to a decrease in lift force of 58.9 N, which represents 1.4% of the total flight weight. Initially, this loss of lift was temporarily compensated for by the reactive force generated by the outflowing air jet. However, once the acceleration phase concluded, the reduction in lift became evident, and the burner needed to be activated to sustain the desired flight altitude. During the experiment, the change in lift due to the acceleration of the balloon led to a descent. Maintaining the balloon at a constant altitude was a difficult task for the pilot. In real flight conditions with a propeller drive, there would be no strict requirement to maintain a constant altitude, meaning the pilot would be able to perform vertical control.

5. MODELING THE DYNAMICS OF THE BALLOON MOTION

Based on the experimental data, the dynamics of balloon motion under the influence of a propulsion system can be analyzed. This information enables the formulation of design requirements for the propulsive unit and the evaluation of the balloon's maneuverability with the selected drive parameters. The force distribution acting on the balloon during horizontal propulsion is illustrated in Fig. 7. The basket was subjected to inertial force, gravitational force (weight), and horizontal thrust, while the balloon envelope was influenced by weight, inertial forces, aerodynamic drag, and static lift.

The interaction between the balloon and the basket was characterized by the force F_b, which represents the result of all forces acting on both components. Of particular interest is the horizontal component of F_b, as it governs the horizontal acceleration of the balloon. This component depends on the inclination angle of the balloon. At the initial moment of actuator activation, no horizontal force component acted on the balloon; only the basket began to accelerate. As the balloon tilted due to the applied thrust, an increasing portion of the propulsion force was transferred to the envelope through the connecting structure.

The equations of motion of the balloon and the basket in the horizontal plane can be written in the following form:

$$T - m_k \frac{dv_k}{dt} - F_{bx} = 0 \ , \tag{10}$$

$$F_{bx} - m_b \frac{dv_b}{dt} - D_b = 0 \ , \tag{11}$$

$$F_{bx} - m_k g \ tg\gamma = 0 \ , \tag{12}$$

$$\gamma = arcsin\left(\frac{x_k - x_b}{l}\right), \tag{13}$$

where:
T – horizontal thrust (N),
m_k – mass of the basket with payload, the balloon burner, and the fuel system (kg),
m_b – total mass of the balloon, including fabric, hot air, and virtual mass of surrounding air (kg),
v_k – horizontal airspeed of the basket (m/s),
F_{bx} – projection of the interaction force of the balloon and the basket on the horizontal plane (N),
t – time (s),
γ – inclination angle of the balloon (rad),
x_k – horizontal coordinate of the basket center (m),
x_b – horizontal coordinate of the balloon center (m),
l – distance between centers of balloon and basket (m).

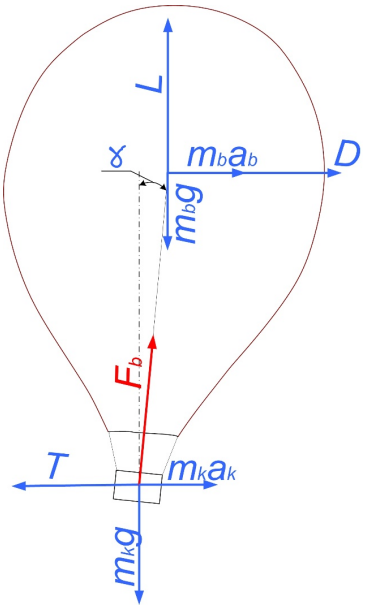

Fig. 7. Scheme of forces acting on the balloon when a horizontal force was applied

Equations (10) and (11) show the balance of horizontal forces acting on the basket and the balloon, respectively. The balance of vertical forces on the basket allowed us to formulate Equation (12). Equation (13) shows the dependence of the angle of inclination of the balloon on the linear parameters. The weight of the balloon is the significant value in those equations, since it takes into account the weight of the fabric, the air inside the balloon, and the virtual mass of the surrounding air. Heat transfer between the air inside and outside the balloon was not considered in the calculations. The density of the air outside was taken according to the ISA at an altitude of 0. According to the calculations, the density of the air inside should correspond to 0.99 kg/m^3. The virtual mass was taken to be the mass of half the air displaced by the balloon [15].

The calculation results are shown in Fig. 8. During the simulation, the acceleration time was determined when the drive was turned on with different thrusts. Fig. 8a shows the simulated acceleration of the balloon to the maximum flight speed with the constant thrust propulsion drive of 486 N. The acceleration time was about 23 s. This value is significant for landing conditions in confined areas. The acceleration of the balloon was accompanied by oscillations with frequencies similar to those obtained in the experiments with the balloon (0.13 Hz).

The possibility of installing a drive with greater thrust (600 N) was considered to reduce acceleration time. It can be turned on at full thrust for a short time for the fastest acceleration of the balloon only. However, the results show that large speed fluctuations can arise in this case, which could

lead to a dangerous convergence of the burner and the fabric. In this regard, we decided against considering this option for the propulsion drive system.

We also considered a lower thrust drive option (250N), as shown in Fig. 8b. In this case, the aircraft had a lower stable flight speed. This option offers improved safety, and it can be used not only for landing but also for some flight modes in free air. The acceleration time increased to 35 s.

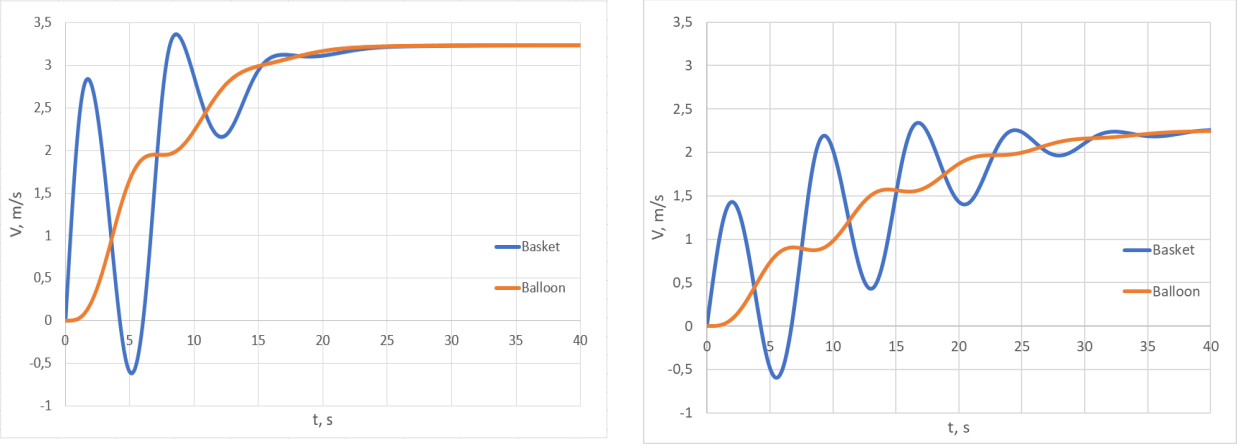

Fig. 8. Calculated velocities of horizontal motion of the balloon and basket based on the results of experiments for the propulsion drive system for (a) 486 N and (b) 250 N

6. CONCLUSIONS

The results allowed us to determine the parameters of the horizontal drive, which can be used to accelerate or brake the balloon in conditions of necessity of landing in confined areas.

The experiments were conducted using a hot-air balloon with a maximum diameter of 14 m and an internal volume of 1.840 m³. The total take-off mass of the balloon system was about 430 kg. Lateral motion was induced by applying a side force, which was measured using the load cell. At high Reynolds numbers, the experimentally determined lateral drag coefficient was 0.35.

Complementary ANSYS simulations of the flow around the balloon confirmed the experimental aerodynamic data. The aerodynamic drag coefficient required for horizontal movement of the balloon was estimated at 0.36. This value differs significantly from those typically reported for spherical objects and high-pressure balloons.

A lateral force of approximately 500 N was required to sustain steady lateral motion at maximum speed. During testing, the balloon reached a maximum airspeed of 3.4 m/s. Further increasing the speed created a risk of damage to the balloon envelope due to the proximity of the burner flame.

The experiments also confirmed that the freely suspended balloon–basket system behaves as an oscillatory structure. When subjected to an external force, the system exhibits pendulum-like motion and requires a finite stabilization time before reaching steady-state conditions.

Under horizontal airflow, the balloon does not behave as a rigid structure but deforms in response to dynamic pressure. This deformation resulted in a 4.5% reduction in the longitudinal depth of the balloon and a 20- to 30-m³ decrease in internal air volume. Consequently, the lift force was reduced by approximately 60 N, equivalent to 1.4 % of the total flight weight. The burner system needs to be activated to compensate for this loss.

The modeling of the balloon's dynamics, based on experimentally measured values, demonstrated that a horizontal propulsion system with a thrust of $T = 486$ N allowed the balloon to reach its maximum horizontal speed only within 23 s. When landing in a confined space, the pilot must take this time into account. Increasing the thrust requires a corresponding increase in the propeller diameter and a more powerful engine, which would increase the weight and complexity of the system. At the same time, a more powerful system can cause the burner to damage the balloon fabric if an unqualified pilot exceeds

the maximum flight speed. Using a propulsion drive with a thrust of 250 N allows a longer motor flight, even if the energy capacity is small. In this case, the propulsion speed will be slightly more than 2 m/s. The acceleration of the balloon was accompanied by oscillations, which, according to the calculations, have a frequency similar to those obtained in experiments with the full-scale balloon (0.13 Hz).

References

1. Aaron, K.M. & Heun, M.K. & Nock, K.T. A method for balloon trajectory control. *Advances in Space Research*. 2002. Vol. 30(5). P. 1227-1232. DOI: 10.1016/S0273-1177(02)00526-4.
2. Almedeij, J.H. Drag coefficient of flow around a sphere: matching asymptotically the wide trend. *Powder Technology*. 2008. Vol. 186(3). P. 218-223. DOI: 10.1016/j.powtec.2007.12.006.
3. Cameron, J. & Smith, I.S. & Cutts, J.A. et al. Versatile modeling and simulation of Earth and planetary balloon systems. In: *International Balloon Technology Conference*. Norfolk: American Institute of Aeronautics and Astronautics. 1999. DOI: 10.2514/6.1999-3876.
4. Carvill, J. *Mechanical Engineer's Data Handbook*. Butterworth-Heinemann. 1993. 342 p.
5. Conrad, G.R. & Robbins, E.J. Determination of balloon drag. In: *International Balloon Technology Conference*. Albuquerque: American Institute of Aeronautics and Astronautics. 1991. DOI: 10.2514/6.1991-3666.
6. Cross, R. & Lindsey, C. Measuring the drag force on a falling ball. *The Physics Teacher*. 2014. Vol. 52(3). P. 169-170. DOI: 10.1119/1.4865522.
7. Daidzic, N.E. Mathematical model of hot-air balloon steady-state vertical flight performance. *Aviation*. 2021. Vol. 25(3). P. 149-158. DOI: 10.3846/aviation.2021.15330.
8. Daidzic, N.E. Mathematical model and simulation of free balloon liftoff in the presence of surface winds. *Aviation*. Vol. 26(1). P. 22-31. DOI: 10.3846/aviation.2022.16621.
9. Dolya, S.N. Payload balloon rising. *Journal of Physics: Conference Series*. 2019. Vol. 1410. No. 012123.
10. Dorrington, G.E. Buoyancy estimation of a Montgolfière in the atmosphere of Titan. *Aeronautical Journal*. 2013. Vol. 117. No. 1195. P. 943-957. DOI: 10.1017/S0001924000008605.
11. Furfaro, R. & Lunine, J.I. & Elfes, A. et al. Wind-based navigation of a hot-air balloon on Titan: a feasibility study. In: *Proceedings of SPIE – Space Exploration Technologies*. Orlando. 2008. Vol. 6960. No. 69600C. DOI: 10.1117/12.777654.
12. Kayhan, Ö. & Hastaoglu, M.A. Modelling of stratospheric balloon using transport phenomena and gas compress-release system. *Journal of Thermophysics and Heat Transfer*. 2014. Vol. 28(3). P. 534-541. DOI: 10.2514/1.T4271.
13. Koran, A. *LDF Powered Balloon Program.* Air Force Cambridge Research Laboratories. 1973. 46 p. Available at: https://apps.dtic.mil/sti/tr/pdf/AD0768673.pdf.
14. Morrison, F.A. *Data correlation for drag coefficient for sphere*. Michigan Technological University. 2013. Available at: https://pages.mtu.edu/~fmorriso/DataCorrelationForSphereDrag2016.pdf.
15. Newman, J.N. *Marine Hydrodynamics. 40th Anniversary Edition*. MIT Press. 2018. 416 p.
16. Rikhlov, A.B. Laws of change of average speed of the wind with height in the ground layer of atmosphere on South-East European part of Russia for the decision of problems wind power. *Uchenye Zapiski RGGMU*. 2011. No. 20. P. 89-100.
17. Sun, Q. & Lim, K.M. & Lee, H.P. & Khoo, B.C. Air drag on a stratospheric balloon in tropical regions. In: *Academic High Altitude Conference*. 2015. DOI: 10.31274/ahac.5572.
18. Taylor, J.A. *Principles of Aerostatics: The Theory of Lighter-Than-Air Flight*. CreateSpace. 2014. 200 p.
19. Tian, Y. & Lin, G. & Guo, J. Drag crisis analysis of a high-altitude balloon in critical transition. *Aerospace Science and Technology*. 2023. Vol. 139. No. 108396. DOI: 10.1016/j.ast.2023.108396.

20. Zhu, R. & Wang, S. & Yang, Y. et al. Design and ground test of a 6 meters pumpkin super-pressure balloon. *Transactions of the Japan Society for Aeronautical and Space Sciences, Aerospace Technology Japan*. 2019. Vol. 17(1). P. 62-67. DOI: 10.2322/tastj.17.62.
21. *Vectored thrust you can trust*. Available at: https://www.flydoo.fun/vtu.

Received 05.07.2024; accepted in revised form 16.02.2026